Int. J. Electrochem. Sci., 10 **(2015)** 552 - 563

International Journal of
ELECTROCHEMICAL
SCIENCE
www.electrochemsci.org

Electrochemical Investigation of the Galvanic Corrosion of AM60 and AD62 Magnesium Alloy in 0.1 M NaCl Solution

Magdalene Edet Ikpi[1,2,*], *Junhua Dong*[2], *Wei Ke*[2]

[1] Corrosion and Electrochemistry Research Group, Department of Pure and Applied Chemistry, University of Calabar, P.M.B. 1115, Calabar, Nigeria.
[2] State Key Laboratory for Corrosion and Protection, Institute of Metal Research, Chinese Academy of Sciences, Shenyang 110016, China.
[*]E-mail: meikpi@chem.unical.edu.ng

Received: 6 October 2014 / *Accepted:* 25 November 2014 / *Published:* 2 December 2014

The corrosion behaviour of AM60 and AD62 magnesium alloy in 0.1 M NaCl solution was investigated by potentiostatic polarisation measurements. The microstructure was evaluated using XRD and SEM. Cathodic hydrogen evolution, NDE, anodic dissolution of magnesium, the formation of magnesium hydride and possibly aluminium hydride were all restrained with Cd addition (AD62 alloy). The presence of Cd in AD62 alloy suppresses the micro-galvanic couple effect existing between α and secondary phases in the alloy, and increases the polarisation resistance arising from the sum effect of the reduced current densities of all anodic and cathodic reactions.

Keywords: Magnesium alloy, Galvanic corrosion, Potentiostatic, Polarisation, SEM, Anodic dissolution

1. INTRODUCTION

Over the years, interest in magnesium alloys has continued to increase due to their potential applications in the automobile, aerospace, electronic and communication industry. Their high strength-to weight ratio, good diecastability, high ductility, high thermal and electrical conductivity and desirable mechanical properties make them the preferred materials for these applications. Yet, they are vulnerable to local corrosion under certain environmental conditions [1-3]. The poorly protective nature of the passive films on Mg alloys [4,5] and the presence of impurities and secondary phases acting as micro-cathodes, result in local galvanic acceleration of corrosion [4] limiting their widespread application.

Significant improvement in the corrosion resistance of Mg can be achieved through alloying [6-8]. The alloyed materials subdue the micro-galvanic effect between α-Mg and the secondary phases [9]. Also, the formation of a stable passive film, based on an oxide of the alloying element provides better corrosion resistance than the magnesium-based oxide or hydroxide; or a different second phase that is more passive and having a greater corrosion resistance than the β-phase may emerge [10].

The AM-series is one of the widely used commercial magnesium alloys. Its corrosion resistance is highly dependent on the level of the impurity elements of Fe, Ni, Cu, and Co. Their high purity variants show similar corrosion rates to high purity Mg [11-13]. Although reports [14,15] have shown enhanced corrosion behaviour with increasing Al concentrations in Mg-Al alloys, the mechanism and role of Al remains unclear. In Mg-Al alloys, Al is partly in solid solution and partly precipitated as β-$Mg_{17}Al_{12}$ phase along the grain boundaries. The β-$Mg_{17}Al_{12}$ phase is passive over a larger pH range compared to its constituent elements (i.e. Al and Mg) [16] and the distribution of the $Mg_{17}Al_{12}$ phase determines the corrosion performance of Mg-Al alloys. The β phase can either accelerate the corrosion process by acting as a galvanic cathode or by inhibiting the corrosion, behaving as an anodic barrier [2,17,18]. Manganese is introduced as an alloy element, usually < 1 wt.% [19] and plays the role of reducing the detrimental effect of iron on the corrosion resistance through the formation of Al-(Fe, Mn) intermetallic particles in the melt [20].

In this work, the corrosion resistance behaviour of AM60 and AD62 magnesium alloys is studied in 0.1 M NaCl solution. Potentiostatic polarisation experiments were employed to study in detail the influence of Cd on the cathodic and anodic processes of AM60 alloy as well as using microscopic techniques to assess the different phases and their impact on the corrosion properties of the alloy.

2. EXPERIMENTAL

2.1 Materials and sample preparation

As-cast Mg-Al-Mn alloy (AM60) and Mg-Al-Mn alloy containing 2 wt.% cadmium (AD62) were used for the study. The chemical composition of these alloys in weight percentage (wt.%) as analysed by inductively coupled plasma atomic emission spectroscopy (ICP-AES) is shown in Table 1.

Table 1. Chemical composition of the alloys

Alloy	Composition (wt.%)							
	Al	Mn	Zn	Si	Fe	Cu	Ni	Cd
AM60	5.91	0.36	< 0.01	0.04	< 0.01	< 0.005	< 0.01	--
AD62	6.44	0.40	< 0.01	0.04	< 0.01	< 0.005	< 0.01	1.88

The specimens for the electrochemical measurements were encapsulated in epoxy resin with about 1 cm^2 of surface area exposed. The surfaces of the epoxy mounted samples were mechanically

ground with silicon carbide paper to 2000 grit. The sample surfaces were cleaned with distilled water and acetone and dried in cold air. An etching reagent of 4 ml of 4 % HNO_3 + 96 ml ethanol was used to reveal the general microstructure of AM60 and AD62 alloys. The corrosion behaviour was studied in 0.1 M NaCl solution and all solutions were prepared using A.R. grade chemicals and distilled water.

2.2 Surface characterisation

The microstructure was investigated using a Philips XL30 Scanning Electron Microscope (SEM). X-ray diffraction technique was employed to determine the constituent phases in the alloys using a D/Max-2500PC XRD machine ($\lambda_{Cu\ Ka}$ = 1.54 Å) with a 2θ scan range of 10 °- 90 °. The grain size was determined by use of a metallurgical microscope.

2.3 Electrochemical tests

Potentiostatic experiments were carried out to simultaneously measure the current density decay and the volume of hydrogen gas evolved using an experimental set up as described by Chen et. al. [21]. A three-electrode system was employed with a Pt plate as auxiliary electrode, a saturated calomel electrode (SCE) as the reference electrode and the sample with 1 cm^2 exposed area as the working electrode. The corrosive medium was 0.1 M NaCl solution with a pH of 7 and the measurements were made at a room temperature of 20 °C. A Model 273A Potentiostat/Galvanostat was used to apply a voltage from -2.4 V/SCE to -0.7 V/SCE. The current density and hydrogen volume produced at each applied potential was measured with time for 1200 s. A 10 ml graduated pipette was employed for the hydrogen volume measurement and estimations in the readings were made to the nearest 0.02 ml.

3. RESULTS

3.1 Microstructure

The microstructure was examined by XRD and the peaks associated with different phases have been assigned as shown in Fig. 1. XRD peaks of α-Mg, $Mg_{17}Al_{12}$ and AlMn phases were clearly identifiable in both alloys. Both AM60 and AD62 are seen to be structurally the same.

The metallographs of representative specimens of AM60 and AD62 are shown in Fig. 2a and 2b respectively. The grain sizes in both alloys were approximately 70-150 μm and precipitates were observed both at grain boundaries and in the grains for both alloys. Likewise, dark, winding contrast portions can be seen along the grain boundaries. These are the defects in the alloys.

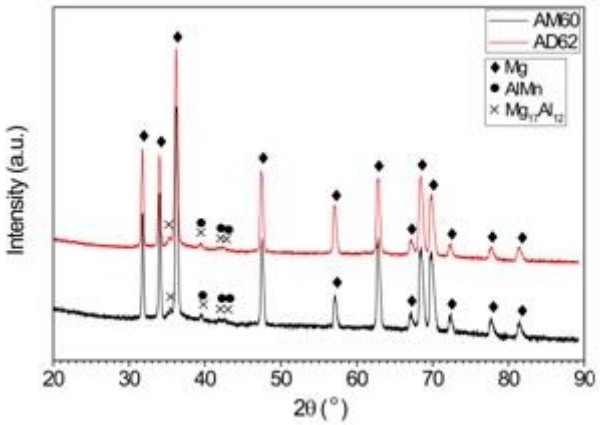

Figure 1. X-ray diffraction patterns of AM60 and AD62 magnesium alloys.

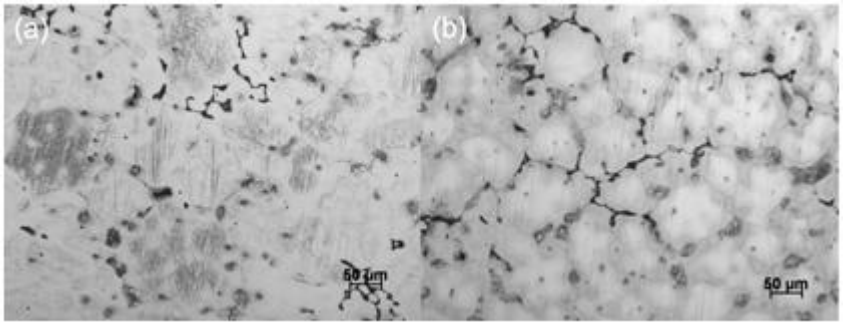

Figure 2. Metallography of (a) AM60 and (b) AD62 alloys showing their general microstructure.

3.2 Corrosion morphologies

The SEM images of AM60 alloy after 24 hrs immersion in 0.1 M NaCl solution is shown in Fig. 3a-3a‴. The surface is characterised by a discontinuous precipitation in lamellar form of β-phase ($Mg_{17}Al_{12}$), appearing mostly at the grain boundaries [17,22,23] with AlMn intermetallic particles (white contrast particles) randomly distributed. The β-phase can exist in the lamellar eutectic phase or in the divorced eutectic phase. A higher magnification image of AM60 (Fig. 3a′) show the lamellar eutectic $Mg_{17}Al_{12}$ β-phase and the divorced eutectic phase which forms under non-equilibrium solidification conditions. Metastable eutectic has been reported to be present in the as-cast microstructure of Mg-Al alloys having more than about 2 wt.% Al [24]. When subjected to an annealing or heat treatment process, the eutectic phase is capable of disappearing and can be completely dissolved in the Mg matrix [25]. The AlMn phase is considered more detrimental than the $Mg_{17}Al_{12}$ phase as the corrosion potential of its pure phase of -1.28 V/SCE after 3 hrs immersion in ASTM D1384 water is higher than that of $Mg_{17}Al_{12}$ phase of -1.31 V/SCE [26]. The corrosion potential for the pure phase of Mg reported for the same study was -1.55 V/SCE. Hence, the extent of corrosion due to the galvanic couple at the Mg matrix/AlMn interface will be more severe than at the Mg matrix/$Mg_{17}Al_{12}$ phase interface as the driving force is large according to the difference between the corrosion potentials. Signs of the deleterious effect of AlMn particles can be seen in the loss of

material around the AlMn particle located in the cavities (discussed later in this section) of Fig. 3b in contrast to the relatively unaffected surface areas surrounding the lamellar $Mg_{17}Al_{12}$ phase (Fig. 3a′ and 3b′). Fig. 3a also reveals the presence of defects resulting from the cast process, and is described here as groove-like features. Pits are seen to appear in near proximity to these defects, which grow deeper and laterally resulting in a large area of material destruction (Fig. 3a″). The pits are irregularly shaped having depths of about 60-300 μm as revealed in the cross-section image of the alloy (Fig. 3a‴). The diameter of the interior of the pit is larger than its orifice.

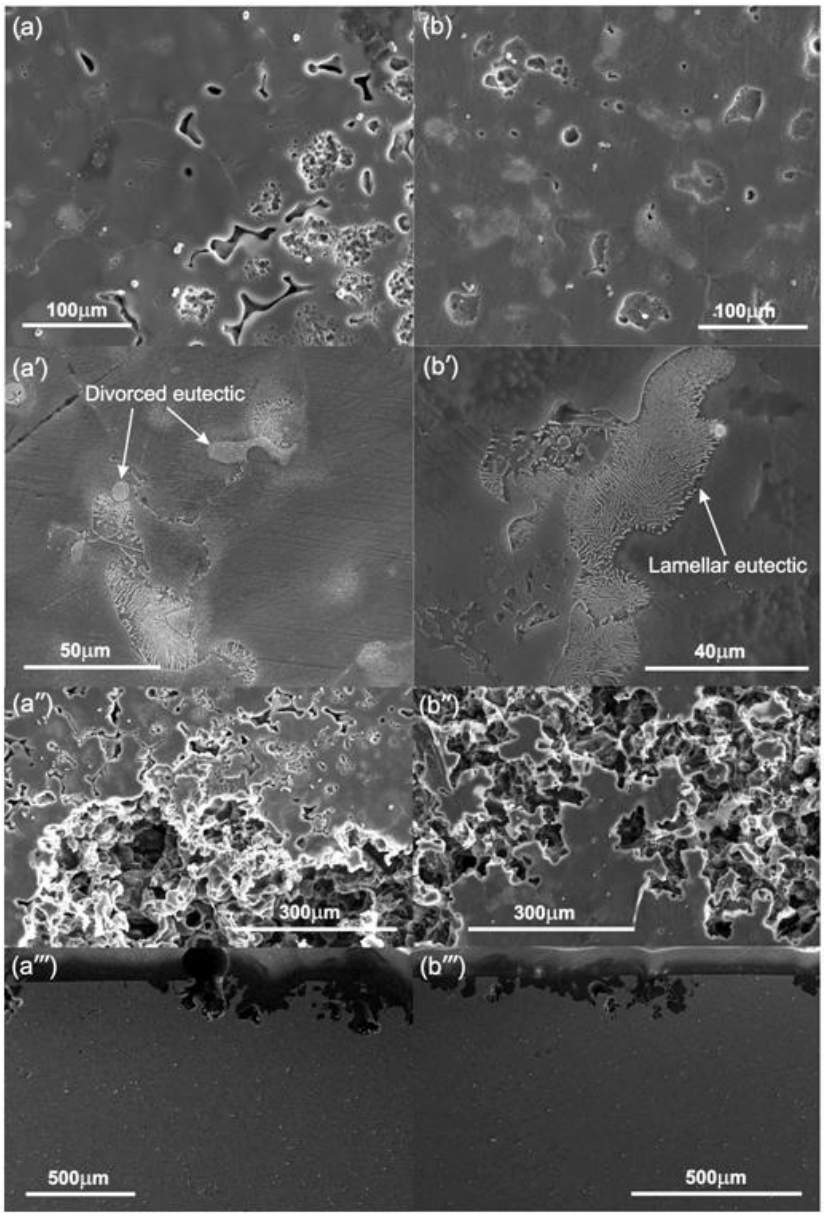

Figure 3. SEM images showing (a) - AM60 alloy and (b) - AD62 alloy after 24 hrs immersion in 0.1 M NaCl solution. (a′), (a″) and (a‴) are the β-phase at the grain boundary, the heavily corroded areas and the cross-section images for AM60 alloy respectively. (b′), (b″) and (b‴) are the β-phase at the grain boundary, the heavily corroded areas and the cross-section images for AD62 alloy respectively.

Fig. 3b-3b‴ show the SEM images of AD62 alloy after 24 hrs immersion in 0.1 M NaCl solution. Features similar to AM60 namely, lamellar eutectic β-phase, the divorced eutectic and the AlMn phases can be seen. Electron Probe Micro-Analyzer (EPMA) images [27] revealed an even distribution of Cd in the uncorroded specimen with no obvious segregation even for the corroded specimens inferring that Cd solidified completely in the single phase α-Mg solid solution. A distinguishing feature observed is the appearance of surface eroded-like areas appearing as cavities of lateral size typically between 20-100 μm and situated roughly within the grain interior. The onset of these pits can be seen on the top left-hand and bottom right-hand corner of Fig. 3b′. A high magnification image of this feature is shown in Fig. 4. These cavities occur due to preferential corrosion of the primary α of the grain interior. Located in some of these cavities are the AlMn intermetallic particles. Zeng et. al. [28] reported that corrosion pits occurred in the area directly surrounding the AlMn particles. The particle acts as a corrosion nucleus, which finally results in an occlusion cell or hemi-spherical corrosion pit similar to the pits in Fig. 3a‴ and 3b‴. Evidence of localised pitting corrosion is also observed on AD62 alloy (Fig. 3b″), though less severe. The depths of the pits are about 30-100 μm and are much shallower (Fig. 3b‴) than the pits in AM60 alloy.

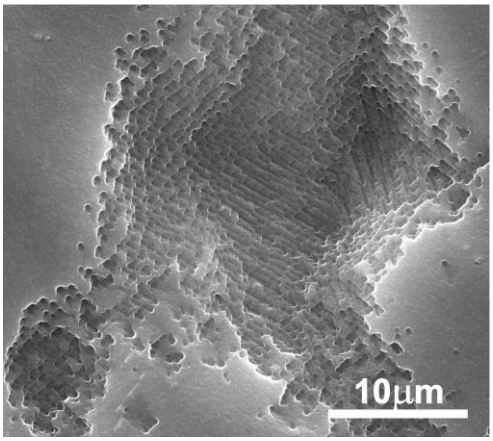

Figure 4. A high magnification image of a shallow pit resulting from corrosion attack of the grain interior of AD62 alloy.

3.3 Potentiostatic polarisation current decay tests

The results for the potentiostatic polarisation experiments for AM60 and AD62 alloys in 0.1 M NaCl solutions are presented in Fig. 5 and Fig. 6 respectively. The plots show the current density decaying to a constant value after about 900 s for each applied potential. The current density increases with increase in the applied anodic potential and decreases with enhancing cathodic polarised potential in both Fig. 5 and 6. The volume of hydrogen gas evolved at each potential increases linearly with time. In addition, the volume of the evolved gas increases with increasing anodic potential and with decreasing cathodic potential. These results are in agreement with previous work [21,29]. By visual inspection, the surface of the specimens showed severe deterioration with increasing applied potential and an increased anodic dissolution rate could be inferred from the increased damage with increasing

anodic polarisation. On the contrary, the surface of the specimens remained unchanged with a slightly tarnished appearance in the cathodic polarisation range.

The gas volumes evolved at each applied potential can be converted to its corresponding current density value using Faraday's law if the assumption that the hydrogen gas evolved obeys the ideal gas model. The current density obtained by this procedure is regarded as the calculated current density. The current density measured by the potentiostat is referred to as the measured or total current density. It is obtained by integrating the area under the average curve gotten from 2-3 different potentiostatic polarisation current decay measurements for each applied potential and dividing the value by the time of measurement. The calculated current density under anodic polarisation (i_{H_2a}) is due to the anodic hydrogen evolution otherwise known as the negative difference effect (NDE) whereas the calculated current density obtained under cathodic polarised conditions (i_{H_2c}) is associated with cathodic reduction of hydrogen ions. The difference observed between the total (measured) current density and the calculated current density under anodic and cathodic polarisation implies that there are other processes occurring. These are the anodic dissolution process of magnesium in the alloy and the cathodic reduction process of magnesium hydride formation [21,29]. An additional cathodic reduction reaction is probably the formation of aluminium hydride.

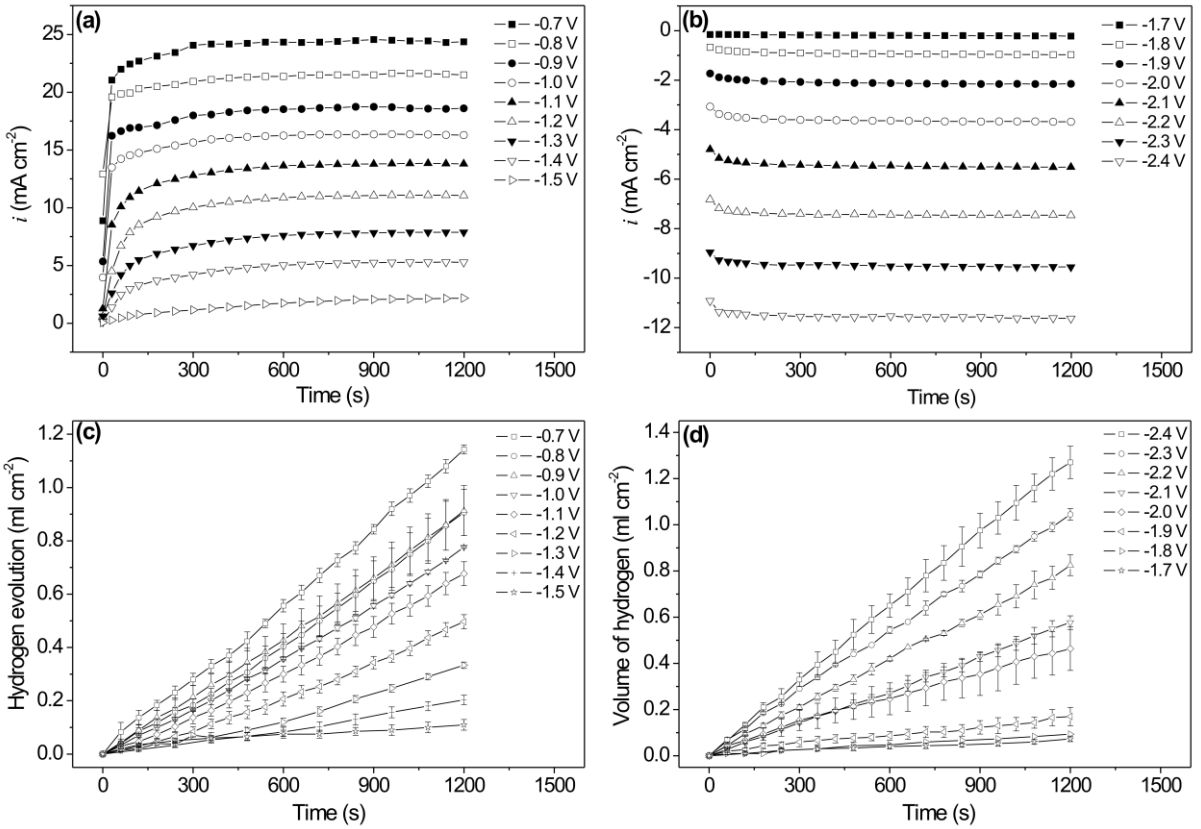

Figure 5. Plots (a) and (b) show the variation of current density with time; (c) and (d) show the volume of hydrogen gas evolved with time for AM60 alloy at different applied potentials in 0.1 M NaCl solution. Plots (a) and (c) represent the anodic process while (b) and (d) represent the cathodic process.

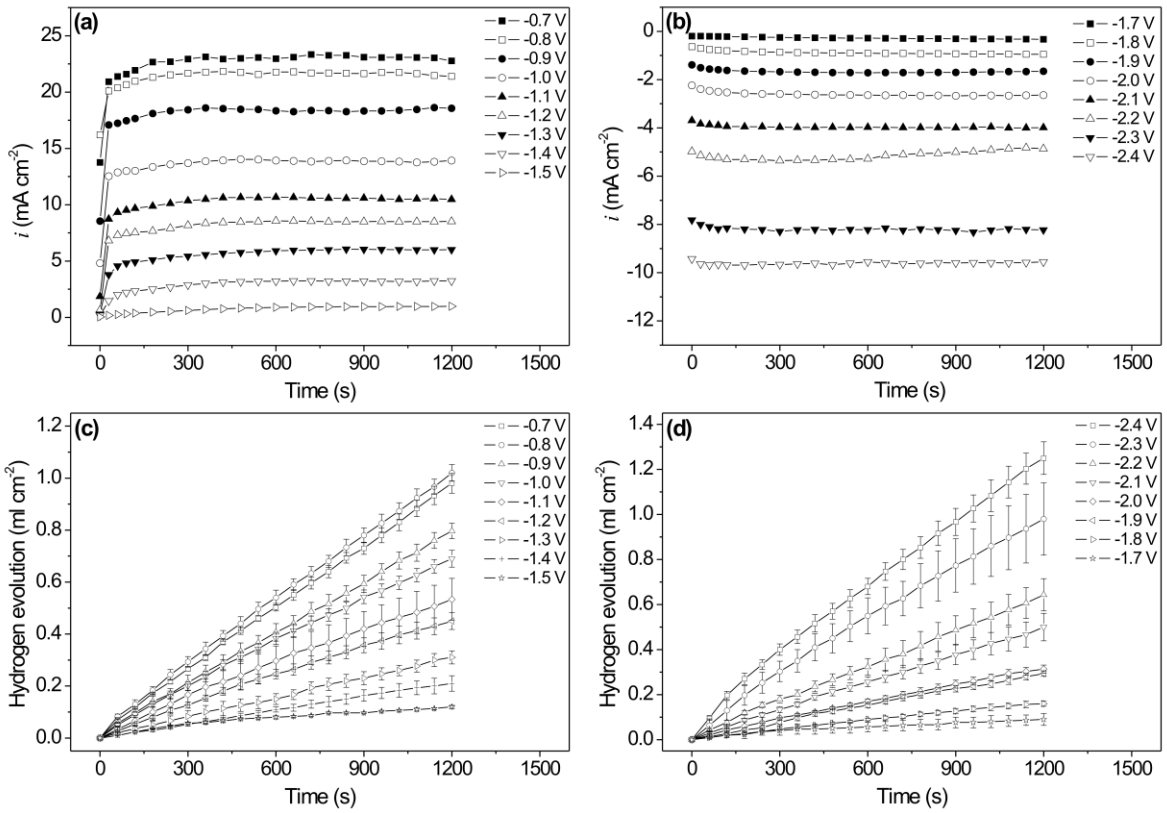

Figure 6. Plots (a) and (b) show the variation of current density with time; (c) and (d) show the volume of hydrogen gas evolved with time for AD62 alloy at different applied potentials in 0.1 M NaCl solution. Plots (a) and (c) represent the anodic process while (b) and (d) represent the cathodic process.

The polarised curves for AM60 and AD62 alloys displaying the measured current densities (i_{meas}), the calculated current densities (i_{calc}) and the difference in the measured and calculated current densities (i_{meas}-i_{calc}) at each applied potential are shown in Fig. 7.

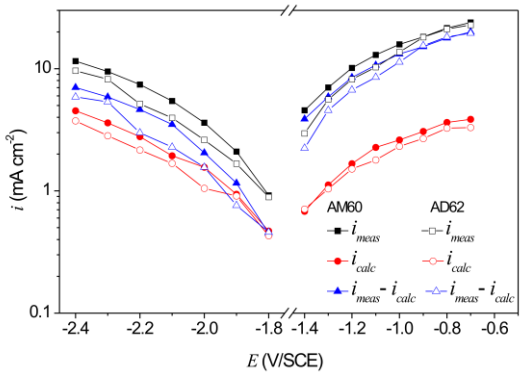

Figure 7. The polarisation curves of AM60 and AD62 alloys in 0.1 M NaCl solution showing the measured current densities (i_{meas} i.e. i_a and i_c), the calculated current densities (i_{calc} i.e. i_{H_2a} and i_{H_2c}) and the difference in the measured and calculated current densities (i_{meas} and i_{calc}).

The measured current densities for AD62 alloy is observed to be lower than the measured current densities for AM60 alloy at both anodic and cathodic polarised conditions with exception for higher anodic polarised conditions (-0.9 V/SCE and above) where the measured current densities for both alloys are comparable. Both the cathodic current density and anodic current density associated with hydrogen release is lower for AD62 than AM60 alloy. The current density arising from the difference in the measured and calculated current densities, i_{meas}-i_{calc} at both cathodic and anodic polarisations show a marked decrease for AD62 compared with AM60, except for higher anodic polarisations of -0.9 V/SCE and above where the values for both alloys are similar.

4. DISCUSSION

The potentiostatic polarisation measurements provide an insight into the relationship between the current densities responsible for the cathodic and anodic hydrogen evolution reactions and the measured or total current density at relatively high anodic and high cathodic polarised potentials. The anodic current density can be regarded as the sum of the current densities for the anodic dissolution process i_{Mg}, and the anodic hydrogen evolution process (NDE) i_{H_2a}. Similarly, the cathodic current density is assumed to be the sum of the current density for the cathodic hydrogen evolution i_{H_2c}, and the current density arising from magnesium hydride formation i_{MgH_2}. In addition, a possible contribution to the measured cathodic current density may arise from the formation of aluminium hydride. Detail expressions for the anodic and cathodic current densities are described in Xu et. al. [29].

Under anodic polarisation, dissolution of Mg is always accompanied by the evolution of hydrogen gas [1,17,30]. The increase in hydrogen evolution rates with increasing applied potential indicates negative difference effect (NDE). The anodic current density measured i_a, is responsible for the anodic dissolution of Mg and the NDE. Thus, the difference between i_a and i_{H_2a} expressed as (i_{meas}-i_{calc}) is the current density due to Mg anodic dissolution. Based on our previous studies [29], the corrosion reactions occurring under anodic polarisation suggests that anodic dissolution proceeds via the monovalent Mg^+ ion [4] as follows;

$$Mg \rightarrow Mg^+ + e^-. \quad (1)$$

$$2Mg^+ + 2H_2O \rightarrow 2Mg^{2+} + 2OH^- + H_2. \quad (2)$$

$$Mg^+ \rightarrow Mg^{2+} + e^-. \quad (3)$$

The anodic dissolution of Mg proceeds through two steps (Eq. 1 and 3). As the potential increases above the pitting potential [4], the rate of the chemical reaction (Eq. 2) increases due to the increased concentration of Mg^+ from Eq. 1. Consequently, there is an increase in hydrogen gas released. From the Pauling scale [31], the electronegativity values for Cd, Al, Mn and Mg are 1.69 eV, 1.61 eV, 1.55 eV and 1.31 eV respectively. On the electronegativity scale, Cd, Al and Mn are

considered more electronegative than Mg, implying that these metals have a stronger affinity for electrons than Mg. Based on the model in our earlier study [29], at conditions of increasing anodic polarisation, Mg acquires a more positive net charge while the other elements become less negatively charged. This is expected to favour an increased anodic dissolution of the Mg matrix (Eq. 1 and 3) in AD62 alloy than AM60 alloy (due to relatively more positive charge on Mg) and a greater inhibition of the reaction of Eq. 2 (due to the stronger electrostatic repulsion between Mg^+ and H^+). However, instead of an increase in the anodic dissolution rate in AD62 alloy, a lower current density is observed for the anodic dissolution process on introducing Cd. The few negative charges on Cd, Al and Mn have the ability to attract H^+ by a weak electrostatic attraction. Despite the attraction, the chemical reaction that results in the formation of hydrogen is further inhibited since all three elements have low exchange current densities (Mn, 1.3 x 10^{-11} A·cm^{-2} < Cd, 1.6 x 10^{-11} A·cm^{-2} < Al, 1.0 x 10^{-10} A·cm^{-2}) [32] for the reduction of H^+ ions; close to the value for mercury (5.0 x 10^{-13} Acm^{-2}). The low hydrogen evolution rate on Hg has been attributed to the nature of its droplet having a very high over potential and a low exchange current density for the reduction of H^+ [33].

The standard thermodynamic data [34] show the equilibrium potential for $E°_{Cd^{2+}/Cd}$ as -0.402 V/SHE, $E°_{Mn^{2+}/Mn}$ as -1.185 V/SHE, $E°_{Al^{3+}/Al}$ as -1.662 V/SHE and $E°_{Mg^{2+}/Mg}$ as -2.372 V/SHE. In AM60 alloy, the α phase is purely Mg and forms micro-galvanic couples principally with β $Mg_{17}Al_{12}$ phase and AlMn phase. In AD62 alloy, the galvanic couples consist of Mg-Cd α-phase and Mg-Al-Cd β-phase. Based on theory, the rate of galvanic corrosion is determined by [35,36] the difference of the rest potentials between the cathode and anode, the cathode and anode polarisation resistance and the solution resistance between the cathode and anode respectively. Cadmium's ability in inhibiting the local corrosion by suppressing the micro-galvanic couple effect is seen in the less damaging effect of galvanic corrosion in both the plan view and cross-sectional images of Fig. 3b″ and 3b‴ and in the reduced corrosion rate based on hydrogen evolution [27]. Our previous work on Mg-Cd alloy system [29] revealed that Cd reduced the cathodic hydrogen evolution, magnesium hydride formation and NDE processes. The introduction of Cd equally restrains all three reactions in addition to inhibiting the anodic dissolution of Mg evidenced by the reduction in the current densities of all anodic and cathodic reactions (Fig. 7). This was attributed to the sum effect of Cd on α-Mg in reducing the cathodic hydrogen evolution, magnesium hydride formation and NDE, and where the effect of all three processes far exceeded the effect of the increase in the anodic dissolution. According to the micro-morphologies of AM60 and AD62 specimens after immersion in the electrolyte solution (Fig. 3), we can say that the potential difference existing in the galvanic couple of AM60 alloy is relatively larger than the potential difference of the galvanic couple of AD62 alloy. Since the distribution of Cd in the alloy is even, it is able to decrease the potential difference between it and other elements and/or phases of the various micro-galvanic cells existing in the alloys. The formation of the second phase (β and AlMn) and the uneven distribution of Al and Mn however, gives rise to the localised corrosion.

Under cathodic polarisation, Eq. 4 occurs as one of the cathodic reactions. Other reactions include the formation of magnesium hydride and aluminium hydride shown in Eq. 5 and 6 respectively.

$$H^+ + e^- \rightarrow ½H_2. \quad (4)$$

$$Mg + 2H^+ + 2e^- \rightarrow MgH_2. \quad (5)$$

$$Al + 3H^+ + 3e^- \rightarrow AlH_3. \quad (6)$$

The Pourbaix diagram of Mg-H_2O and Al-H_2O systems at 20 °C generated using Factsage 6.2 thermodynamic software, shows MgH_2 and AlH_3 at pH 7 existing in these forms at potentials lower than -1.544 V/SCE and -1.524 V/SCE respectively. At potentials higher than these, both MgH_2 and AlH_3 decompose releasing H_2 gas with Mg and Al existing as Mg^{2+} and $Al_2O_3.H_2O$ soluble species.

A decreasing electrode potential results in a more negative net charge on Cd, Al and Mn and a less positive net charge on Mg. A stronger electrostatic attraction of H^+ to Cd, Al and Mn will reduce the probability at which Mg collides with H^+, restraining more the formation of MgH_2 in AD62 alloy than in AM60 alloy. Again, the reduction of H^+ (Eq. 4) will equally be restrained more in AD62 alloy as Cd, possesses a very low exchange current density value for the reduction of H^+. Since the formation of MgH_2 is inhibited more in AD62 alloy, the subsequent release of hydrogen from its decomposition will equally be low. The more negative net charge on Al increases the likelihood of collision between it and H^+ resulting in the formation of AlH_3 (Eq. 6). However, in the Cd-containing alloy, the stronger electrostatic attraction of H^+ to Cd will reduce the probability at which Al collides with H^+, restraining the formation of AlH_3 in AD62 alloy.

5. CONCLUSIONS

The corrosion behaviour of AM60 and AD62 magnesium alloys in 0.1 M NaCl solution was studied using potentiostatic polarisation measurements. Cd, Al and Mn synergistically reduced the anodic dissolution of Mg in AD62 alloy. The presence of Cd in AD62 alloy inhibited both the cathodic and anodic hydrogen evolution process and restrained the magnesium and aluminium hydride formation. The sum effect of these reactions leads to an increase in the polarisation resistance of AD62 alloy. The even distribution of Cd in AD62 alloy suppresses the micro-galvanic couple effect in the alloy, thus enhancing the corrosion resistance of the alloy.

ACKNOWLEDGEMENTS
M. E. Ikpi acknowledges the Chinese Academy of Sciences (CAS) and the Academy of Sciences for the Developing World (TWAS) for the CAS-TWAS Postdoctoral Fellowship.

References

1. G. Song, A. Atrens, D. St John, X. Wu, J. Nairn, *Corros. Sci.* 39 **(**1997) 1981
2. G.L. Song, A. Atrens, *Adv. Eng. Mater.* 1 (1999) 11
3. E. Ghali, *Magnesium and Magnesium Alloys, in: R.W. Revie (Ed), Uhlig's Corrosion Handbook,* John Wiley & Sons Inc., New Jersey, (2000)

4. G. Song, A. Atrens, *Adv. Eng. Mater.* 5 (2003) 837
5. F. El-Taib, Heakal, A.M. Fekry, M.Z. Fatayerji, *Electrochim. Acta* 54 (2009) 1545
6. X. Zhou, Y. Huang, Z. Wei, Q. Chen, F. Gan, *Corros. Sci.* 48 (2006) 4223
7. Y. Ding, C. Wen, P. Hodgson, Y. Li, *J. Mater. Chem. B.* 2 (2014) 1912
8. N. D. Nam, *J. Magnesium Alloys.* 2 (2014) 190
9. R. Arrabal, A Pardo, M.C. Merino, M. Mohedano, P. Casajús, K. Paucar, G. Garcés, *Corros. Sci.* 55 (2012) 301
10. A. Atrens, *Adv. Eng. Mater.* 6 (2004) 83
11. G. Song, *Adv. Eng. Mater.* 7 (2005) 563
12. G. Song, D. St. John, *J. Light Met.* 2 (2002) 1
13. N. Winzer, A. Atrens, G. Song, E. Ghali, W. Dietzel, K.U. Kainer, N. Hort, C. Blawert, *Adv. Eng. Mater.* 7 (2005) 659
14. G.L. Makar, J. Kruger, *J. Electrochem. Soc.* 137 (1990) 414
15. C.B. Baliga, P. Tsakiropoulos, *Mater. Sci. Technol.* 9 (1993) 513
16. O. Lunder, J.E. Lein, T.Kr. Aune, K. Nisancioglu, *Corros.* 45 (1989) 741
17. G. Song, A. Atrens, X. Wu, B. Zhang, *Corros. Sci.* 40 (1998) 1769
18. M. Zhao, M. Liu, G. Song, A. Atrens, *Corros. Sci.* 50 (2008) 1939
19. C.M. Liu, X.Y. Zhu, H.T. Zhou, *Phase Diagrams of Magnesium Alloys*, Zhongnan University Press, Changsha, (2006)
20. G.L. Makar, J. Kruger, *Inter. Mater. Rev.* 38 (1993) 138
21. J. Chen, J. Dong, J. Wang, E. Han, W. Ke, *Corros. Sci.* 50 (2008) 3610
22. O. Lunder, T.Kr. Aune, K. Nisancioglu, *Corros.* 43 (1987) 291
23. C. Suman, *SAE Transact.* 99 (1990) 849
24. D.J. Sakkinen, *Physical metallurgy of magnesium die cast alloys, Attributes of Magnesium for Automobile Design*, SAE, Warrendale, (1994)
25. S. Kleiner, O. Beffort, A. Wahlen, P.J. Uggowitzer, *J. Light Met.* 2 (2002) 277
26. S. Mathieu, C. Rapin, J. Steinmetz, P. Steinmetz, *Corros. Sci.* 45 (2003) 2741
27. M.E. Ikpi, J. Dong, W. Ke: paper submitted for presentation at Corrosion 2014, International Conference, 18-21 Nov. 2014, Gliwice, Poland.
28. R.C. Zeng, J. Zhang, W.J. Huang, W. Dietzel, K.U. Kainer, C. Blawert, W. Ke, *Trans. Nonf. Metals Soc. China* 16 (2006) s763
29. S. Xu, M.E. Ikpi, J. Dong, J. Wei, W. Ke, N. Chen, *Int. J. Electrochem. Sci.* 7 (2012) 4735
30. G. Song, A. Atrens, D. St. John, J. Nairn, Y. Li, *Corros. Sci.* 39 (1997) 855
31. R.S. Evans, J.E. Huheey, *J. Inorg. Nucl. Chem.* 32 (1970) 373
32. H. Wendt, G. Kreysa, *Electrochemical Engineering: Science and Technology in Chemical and Other Industries*, Springer-Verlag, Heidelberg, (1999)
33. H. Kita, *J. Electrochem. Soc.* 113 (1966) 1095
34. M. Pourbaix, *Atlas of Electrochemical Equilibria in Aqueous Solutions*, NACE International, Houston (1974)
35. G.-L. Song, *Corros. Sci.* 52 (2010) 455
36. G. Song, B. Johannesson, S. Hapugoda, D.H. St John, *Corros. Sci.* 46 (2004) 955